High sensitivity gravimetric sensor made of unidirectional carbon fiber epoxy composite on $(1-x)$Pb$(Zn_{1/3}Nb_{2/3})O_3$-xPbTiO$_3$ single crystal substrate*

Huang Nai-Xing(黄乃兴)[a)b)], Lü Tian-Quan(吕天全)[a)†], Zhang Rui(张 锐)[a)‡], and Cao Wen-Wu(曹文武)[a)c)]

[a)] *Condensed Matter Science and Technology Institute, Department of Physics, Harbin Institute of Technology, Harbin* 150080, *China*
[b)] *Department of Physics, College of Electronic Science, Northeast Petroleum University, Daqing* 163318, *China*
[c)] *Materials Research Institute, The Pennsylvania State University, University Park, Pennsylvania* 16802, *USA*

(Received 23 April 2014; revised manuscript received 19 May 2014; published online 24 September 2014)

We have derived a general formula for sensitivity optimization of gravimetric sensors and have used it to design a high sensitivity gravimetric sensor using unidirectional carbon fiber epoxy composite (CFEC) waveguide layer on $(1-x)$Pb$(Zn_{1/3}Nb_{2/3})O_3$-xPbTiO$_3$ (PZN-xPT) single crystal substrate with the carbon fibers parallel to the x_1 and x_2 axes, respectively. The normalized maximum sensitivity $\left(\left|S_{\rm m}^{\rm f}\right|\lambda\right)_{\rm max}$ exhibits an increasing tendency with the decrease of $(h/\lambda)_{\rm opt}$ and the maximum sensitivity $\left(\left|S_{\rm m}^{\rm f}\right|\lambda\right)_{\rm max}$ increases with the elastic constant $c_{66}^{\rm E}$ of the piezoelectric substrate material. For the CFEC/$[011]_c$ poled PZN-7%PT single crystal sensor configuration, with the carbon fibers parallel to the x_1 axis at $\lambda = 24$ μm, the maximum sensitivity $\left|S_{\rm m}^{\rm f}\right|_{\rm max}$ can reach as high as 1156 cm^2/g, which is about three times that of a traditional SiO$_2$/ST quartz structure gravimetric sensor. The better design selection is to have the carbon fibers parallel to the direction of propagation of Love wave in order to obtain the best sensitivity.

Keywords: Love wave, gravimetric sensor, ferroelectric single crystal, sensitivity optimization

PACS: 77.84.–s, 52.35.Mw, 77.65.Dq, 07.07.Df **DOI:** 10.1088/1674-1056/23/11/117704

1. Introduction

Love wave devices have been used in liquids and gases for biochemical applications and gas contamination detections.[1,2] It is known that Love waves exist only when a thin layer is attached on a substrate, and the velocity of the shear wave in the layer must be slower than that in the substrate.[3] At present, almost all Love-mode devices use ST quartz as the substrate material.[1–6] By analyzing gravimetric sensors made of fused quartz, SiO$_2$, polymethylmethacrylate (PMMA), ZnO, etc. as the waveguide layers, a general rule for improving the sensor sensitivity has been summarized: the waveguide material should have low density, low shear velocity, and low acoustic attenuation.[7,8] Although the theoretical maximum sensitivity of a Love wave sensor with a PMMA waveguide layer has reached a very high value because PMMA has low density and low velocity, the theoretical design thickness is not practical because the PMMA material is very lossy.[7,8] Hence, we must search for a waveguide material with a low acoustic absorption loss. The CFEC provides an acoustic impedance comparable to that of aluminum, so that CFEC is a potential waveguide material. In a Love wave device, insertion loss can be reduced by selecting a substrate with larger electromechanical coupling coefficient.[9] In recent years, a new generation of relaxor-PT ferroelectric single crystal materials have been developed, including Pb$(Zn_{1/3}Nb_{2/3})O_3$-xPbTiO$_3$ (PZN-xPT) single crystals, whose piezoelectric effect is five times as high as that of Pb(Ti,Zr)O$_3$ (PZT) piezoelectric ceramics[10] and whose electromechanical coupling factors are better than 85%,[11] which is much larger than that of quartz.[12] In particular, the electromechanical coupling coefficient k_{32} of $[011]_c$ poled PZN-7%PT single crystal reached as high as 0.86 and the piezoelectric constant d_{32} reaches -1460 pC/N at room temperature.[13] The PZN-xPT single crystals possess high electromechanical coefficients, which help to enhance the efficiency of converting electrical energy into mechanical energy (and vice versa). Hence, the sensor performance can be improved due to the increase of the efficiency. For the CFEC/$[011]_c$ poled Pb$(Mg_{1/3}Nb_{2/3})O_3$-0.29PbTiO$_3$ single crystal sensor configuration with carbon fibers parallel to the x_1 axis, we have found that the maximum sensitivity $\left|S_{\rm m}^{\rm f}\right|_{\rm max}$ can reach as high as 1230 cm^2/g.[14] It is expected that a gravimetric sensor made of PZN-xPT single crystal substrate can offer high sensitivity due to the confinement of the acoustic energy to the sensing surface. In order to design higher sensitivity gravimetric sensors, it is important to know the preferred orientation of carbon fibers in the waveguide layer and the optimal design parameters in a specific device configuration.

Partial wave theory is the most commonly used method for analyzing acoustic wave propagation in anisotropic

*Project supported by the National Basic Research Program of China (Grant No. 2013CB632900).
†Corresponding author. E-mail: ltq@hit.edu.cn
‡Corresponding author. E-mail: ruizhang_ccmst@hit.edu.cn
© 2014 Chinese Physical Society and IOP Publishing Ltd

materials.[14–18] In this work, we have derived the dispersion relation of a Love wave by employing partial wave theory for a specific sensor structure using PZN-xPT ($x = 0.045$–0.09) single crystals poled along $[001]_c$ and $[011]_c$ pseudo-cubic directions as substrates. Based on modal analysis and perturbation theory, optimal parameters have been derived for designing a gravimetric sensor with a CFEC waveguide layer (the carbon fibers parallel to the x_1 and x_2 axes, respectively). More importantly, a general design rule to improve the sensitivity of such sensors is presented for the preferred orientation of the fibers in unidirectional waveguide material, as well as the selection of piezoelectric substrate.

2. Theoretical formulas

The guiding layer and piezoelectric substrate are bonded as shown in Fig. 1. This is a basic configuration supporting Love waves without the mass loading layer. The substrates are $Pb(Zn_{1/3}Nb_{2/3})O_3$-(0.045–0.09)$PbTiO_3$ single crystals poled along $[001]_c$ and $[011]_c$ pseudo-cubic directions. The elastic wave equations in the media are given by[19]

$$\rho\frac{\partial^2 u_j}{\partial t^2} - c_{ijkl}\frac{\partial^2 u_k}{\partial x_i \partial x_l} - e_{kij}\frac{\partial^2 \varphi}{\partial x_i \partial x_k} = 0, \tag{1a}$$

$$e_{ikl}\frac{\partial^2 u_k}{\partial x_i \partial x_l} - \varepsilon_{ik}\frac{\partial^2 \varphi}{\partial x_i \partial x_k} = 0, \quad (i,j,k,l = 1,2,3), \tag{1b}$$

where ρ is the density, c_{ijkl} is the elastic stiffness tensor component at constant electric field, e_{kij} is the piezoelectric coefficient tensor component at constant stress, and ε_{ik} is the dielectric permittivity tensor component at constant strain. The particle displacements and the electric potential in the media can be written as

$$u_j = \alpha_j \exp(\mathrm{i}kbx_3)\exp[\mathrm{i}k(x_1 - vt)], \tag{2a}$$

$$\varphi = \alpha_4 \exp(\mathrm{i}kbx_3)\exp[\mathrm{i}k(x_1 - vt)], \tag{2b}$$

where v is the phase velocity, k is the magnitude of wave vector $\boldsymbol{k}$, b is the decay coefficient along x_3, and α's give the relative amplitudes. Since the guiding layer thickness h is finite and the substrate is considered infinite half-space (assuming that the thickness of substrate is much greater than the wavelength λ), the general solution of the displacements and the electric potential can be written as

$$\hat{u}_j = \left\{\sum_n C_n \alpha_j^{(n)} \exp(\mathrm{i}kb^{(n)}x_3)\right\}\exp[\mathrm{i}k(x_1 - vt)], \quad (n = 1,2,\ldots,8), \tag{3a}$$

$$\hat{\varphi} = \left\{\sum_n C_n \alpha_4^{(n)} \exp(\mathrm{i}kb^{(n)}x_3)\right\}\exp[\mathrm{i}k(x_1 - vt)], \quad (n = 1,2,\ldots,8), \tag{3b}$$

$$u_j = \left\{\sum_m C_m \alpha_j^{(m)} \exp(\mathrm{i}kb^{(m)}x_3)\right\}\exp[\mathrm{i}k(x_1 - vt)], \quad (m = a,b,c,d), \tag{3c}$$

$$\varphi = \left\{\sum_m C_m \alpha_4^{(m)} \exp(\mathrm{i}kb^{(m)}x_3)\right\}\exp[\mathrm{i}k(x_1 - vt)], \quad (m = a,b,c,d), \tag{3d}$$

where C_n and C_m are weighting factors of these partial waves in the guiding layer and substrate, respectively. The symbols marked with "$\hat{}$" are parameters of the waveguide layer and are used to distinguish them from that of piezoelectric substrate.

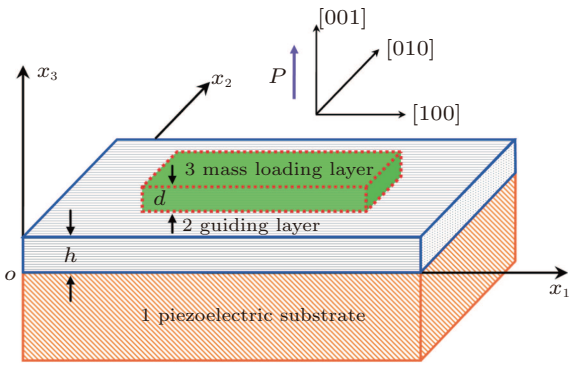


Fig. 1. (color online) Illustration of the sensor design and the coordinate system.

At the surface ($x_3 = h$) of the basic configuration supporting Love waves, the traction must be zero. The particle displacements and the three components of stress tensor must be continuous across the interface ($x_3 = 0$), assuming no slippery interface. The electrical boundary conditions involve the continuity of the electric potential, and the normal component of the electric displacement across both the surface and the interface. In the coordinate system shown in Fig. 1, the boundary conditions of the problem are as follows:

$$x_3 = h: \ \hat{T}_{31} = 0, \ \hat{T}_{32} = 0, \ \hat{T}_{33} = 0, \ \hat{D}_3 = k\varepsilon_0\hat{\varphi}, \tag{4a}$$

$$x_3 = 0: \ u_1 = \hat{u}_1, \ u_2 = \hat{u}_2, u_3 = \hat{u}_3, \ T_{31} = \hat{T}_{31}, \ T_{32} = \hat{T}_{32}, \ T_{33} = \hat{T}_{33}, \varphi = \hat{\varphi}, \ D_3 = \hat{D}_3. \tag{4b}$$

The traction stresses are expressed by

$$T_{3j} = c_{3jkl}(\partial u_k/\partial x_l) + e_{k3j}(\partial\varphi/\partial x_k), \tag{5}$$

and the normal component of the electric displacement is given by

$$D_3 = e_{3kl}(\partial u_k/\partial x_l) - \varepsilon_{3k}(\partial\varphi/\partial x_k). \tag{6}$$

When being poled along $[001]_c$ direction, the PZN-xPT single crystal has a $4mm$ macroscopic symmetry,[20,21] and the macroscopic symmetry is orthorhombic $mm2$ for PZN-xPT single crystal polarized along $[011]_c$.[13,22] Generally, the single crystals in the rhombohedral phase have eight possible spontaneous polarization directions, four orientations remain after being poled along $[001]_c$, as shown in Fig. 2(a), and two orientations remain after being poled along $[011]_c$, as shown in Fig. 2(b). The CFEC with the carbon fibers parallel to the

x_1 and x_2 axes was selected as the waveguide material, respectively. The two CFEC-on-PZN-xPT structures fit the NP53 symmetry.[19] The $[001]_c$ and $[011]_c$ poled PZN-xPT single crystals are used as testing substrates, and the wave propagation is along the x_1 direction in our design. For the carbon fibers parallel to the x_2 axis, namely the fibers perpendicular to the direction of propagation of Love wave, by substituting Eq. (2) and material constants from Table 1, Refs. [13] and [20]–[22] into Eq. (1) and using Eqs. (3)–(6), we can derive the related dispersion equation of Love wave

$$\tan\left\{kh\hat{\delta}\left[(v/\hat{v}_s)^2-1\right]^{1/2}\right\}=\eta\frac{\delta}{\hat{\delta}}\left\{\frac{1-(v/v_s)^2}{(v/\hat{v}_s)^2-1}\right\}^{1/2}, \quad (7)$$

where $\hat{v}_s < v < v_s$ (for exact real solutions of k), $\eta = c_{44}/\hat{c}_{44}$, $\delta = (c_{66}/c_{44})^{1/2}$, $\hat{\delta} = (\hat{c}_{66}/\hat{c}_{44})^{1/2}$, $v_s = \delta(c_{44}/\rho)^{1/2}$, $\hat{v}_s = \hat{\delta}(\hat{c}_{44}/\hat{\rho})^{1/2}$, $k = 2\pi/\lambda$. Using Eqs. (1)–(7), the distributions of Love wave displacements, normalized to the values at the surface ($x_3 = h$), can be expressed as

$$U^{(1)}_{(x_3)} = \cos\left\{k\hat{\delta}\left[(v/\hat{v}_s)^2-1\right]^{1/2}(x_3-h)\right\}, \quad (0\le x_3\le h), \quad (8a)$$

$$U^{(2)}_{(x_3)} = \cos\left\{k\hat{\delta}\left[(v/\hat{v}_s)^2-1\right]^{1/2}h\right\} \times \exp\left\{k\delta\left[1-(v/v_s)^2\right]^{1/2}x_3\right\}, \quad (x_3\le 0). \quad (8b)$$

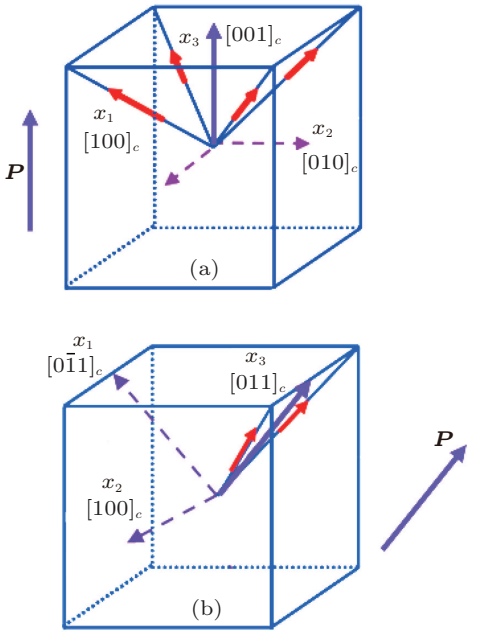


Fig. 2. (color online) Illustration of the polarization of PZN-PT single crystal. (a) Four spontaneous polarization directions remain after being poled along $[001]_c$. (b) Two orientations remain after being poled along $[011]_c$.

Table 1. Material constants of the unidirectional carbon fiber epoxy composite (CFEC) with the fibers parallel to the x_2 axis.[a)]

Elastic constants/10^{10} N·m^{-2}							Density/kg·m^{-3}
c_{11}	c_{12}	c_{13}	c_{22}	c_{44}	c_{55}	c_{66}	ρ
1.37	0.67	0.71	12.6	0.58	0.33	0.58	1580

[a)] Calculated from Table 2 data.

In practical device configuration, a thin mass layer (density ρ_3, shear modulus μ_3, shear velocity v_{S3}, and thickness d) is loaded onto the surface of the guiding layer. Based on the perturbation theory,[24] the relative frequency sensitivity definition for a gravimetric sensor is given by[3,7]

$$S_m^f = \frac{1}{f_0}\lim_{\Delta m_s\to 0}\left(\frac{\Delta f}{\Delta m_s}\right) = \frac{1}{\rho_3 d}\frac{\Delta f}{f_0} = -\frac{(1-v_{S3}^2/v_0^2)}{2\hat{\rho}\Gamma(h)}, \quad (9)$$

where $\Delta f = f - f_0$, f and f_0 are the oscillation frequencies for perturbed and unperturbed cases, respectively, Δm_s is the mass per unit area, and $\Gamma(h)$ is given by

$$\Gamma(h) = \int_h^0 \left|U^{(1)}_{(x_3)}\right|^2 dx_3 + \frac{\rho}{\hat{\rho}}\int_0^{-\infty}\left|U^{(2)}_{(x_3)}\right|^2 dx_3. \quad (10)$$

When the Rayleigh hypothesis is applicable, that is, when the elasticity of the mass loading layer can be ignored ($v_{S3}^2 = \mu_3/\rho_3 = 0$), the equation (9) can be simplified to

$$S_m^f = \frac{-1}{2\hat{\rho}\Gamma(h)}. \quad (11)$$

Substituting Eq. (8) into Eq. (10) and then into Eq. (11) gives the sensitivity formula

$$S_m^f = \frac{-1}{\hat{\rho}h}\left(1+\frac{\sin(\beta_2 h)\cos(\beta_2 h)}{\beta_2 h}+\frac{\rho}{\hat{\rho}}\frac{\cos^2(\beta_2 h)}{\beta_1 h}\right)^{-1}, \quad (12)$$

with $\beta_1 = k\delta[1-(v/v_s)^2]^{1/2}$, $\beta_2 = k\hat{\delta}[(v/\hat{v}_s)^2-1]^{1/2}$, and $k = 2\pi/\lambda = 2\pi f/v$.

For the carbon fibers parallel to the direction of wave propagation that the fibers along the x_1 axis, the material constants of the unidirectional CFEC are listed in Table 2. By substituting Eq. (2) and material constants from Table 2, Refs. [13] and [20]–[22] into Eq. (1), and using Eqs. (3)–(6), we can derive the similar dispersion relation and the sensitivity equation following the steps above.[14]

Table 2. Material constants of the unidirectional carbon fiber epoxy composite (CFEC) with the fibers parallel to the x_1 axis.[23]

Elastic constants/10^{10} N·m^{-2}							Density/kg·m^{-3}
c_{11}	c_{12}	c_{22}	c_{23}	c_{44}	c_{55}	c_{66}	ρ
12.6	0.67	1.37	0.71	0.33	0.58	0.58	1580

3. Results and discussion

The dispersion relations of the Love waves for a CFEC guiding layer on a $[011]_c$ poled PZN-7%PT single crystal substrate structure with the carbon fibers parallel to the x_1 and x_2 axes are shown in Figs. 3 and 4, respectively. Each dispersion curve starts at the shear horizontal (SH) wave velocity (2972 m/s) of the PZN-7%PT single crystal. At this speed, all of the higher-order Love modes have low-frequency cutoffs. At high frequencies, the phase velocities of all Love modes approach asymptotically to the shear wave velocity of 1916 m/s

in CFEC. From Figs. 3 and 4, we found that the dispersion curves distribution in Fig. 4 is wider than that in Fig. 3 for the very different orientations of the carbon fibers. For other composition PZN-xPT ($x = 4.5\%$, 8%, and 9%) single crystal substrates poled along $[001]_c$ and $[011]_c$, we can obtain similar dispersion curves.

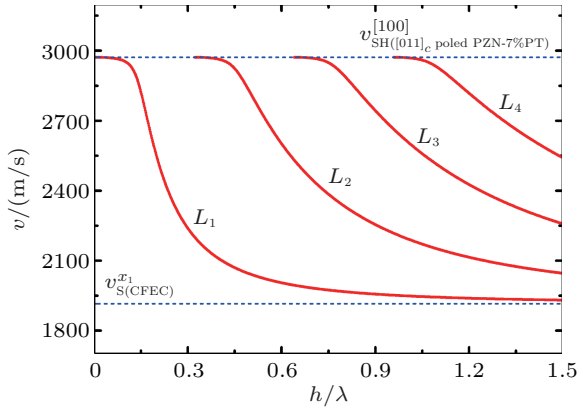


Fig. 3. (color online) Dispersion curves of Love waves for a CFEC/$[011]_c$ poled PZN-7%PT single crystal structure with the carbon fibers parallel to the x_1 axis.

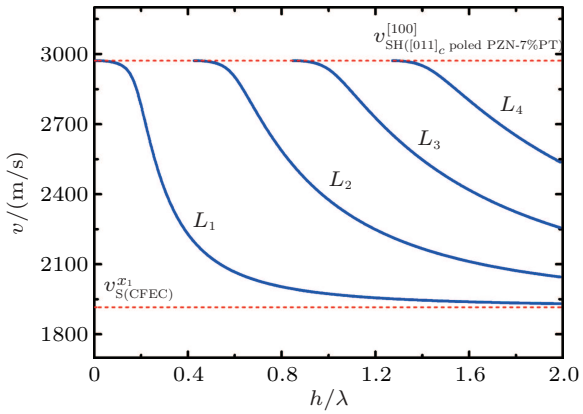


Fig. 4. (color online) Dispersion curves of Love waves for a CFEC/$[011]_c$ poled PZN-7%PT single crystal structure with the carbon fibers parallel to the x_2 axis.

Figures 5 and 6 show the relative frequency sensitivity $\left|S_{\mathrm{m}}^{\mathrm{f}}\right|\lambda$ for the first four modes of the CFEC on $[011]_c$ poled PZN-7%PT structure with the carbon fibers parallel to the x_1 and x_2 axes, respectively. It was found that the first-order mode possesses the highest $\left(\left|S_{\mathrm{m}}^{\mathrm{f}}\right|\lambda\right)_{\max}$, and the changing trend shown in Figs. 5 and 6 is consistent with theoretical expectations. For the sensor design with the carbon fibers parallel to the x_1 axis, the optimal ratio of the guiding layer thickness to the wavelength is: $(h/\lambda)_{\mathrm{opt}} = 0.183$, the normalized maximum sensitivity is: $\left(\left|S_{\mathrm{m}}^{\mathrm{f}}\right|\lambda\right)_{\max} = 2.775$ (10^{-3} $\mathrm{m^3/kg}$), which is about three times that of a traditional fused quartz/ST quartz structure.[3] Because of the wavelength used in Ref. [2] was 24 μm, for the CFEC/$[011]_c$ poled PZN-7%PT configuration, the optimal design parameters are: $h = 4.392$ μm, $f = 109.8$ MHz, and the maximum sensitivity of $\left|S_{\mathrm{m}}^{\mathrm{f}}\right|_{\max} = 1156$ ($\mathrm{cm^2/g}$), which is about three times that of a traditional configuration. In addition, for the sensor design with the carbon fibers parallel to the x_2 axis, the optimal design parameters are: $h = 5.844$ μm, $f = 108.5$ MHz, and the maximum sensitivity of $\left|S_{\mathrm{m}}^{\mathrm{f}}\right|_{\max} = 843$ ($\mathrm{cm^2/g}$) (see Table 3).

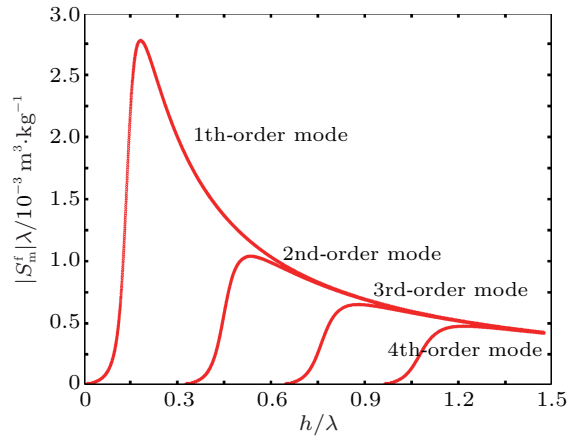


Fig. 5. (color online) Relative scaled frequency sensitivity $\left|S_{\mathrm{m}}^{\mathrm{f}}\right|\lambda$ for the first four modes in a CFEC/$[011]_c$ poled PZN-7%PT single crystal structure with the carbon fibers parallel to the x_1 axis.

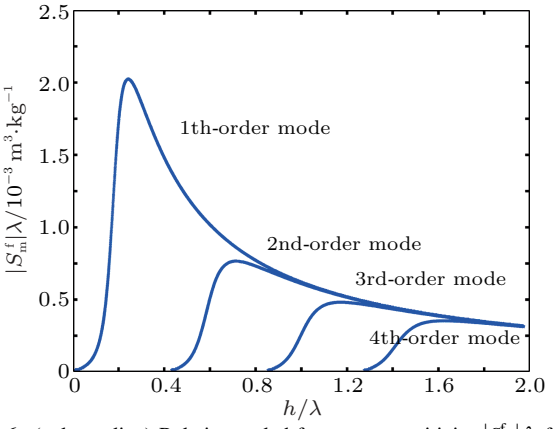


Fig. 6. (color online) Relative scaled frequency sensitivity $\left|S_{\mathrm{m}}^{\mathrm{f}}\right|\lambda$ for the first four modes in a CFEC/$[011]_c$ poled PZN-7%PT single crystal structure with the carbon fibers parallel to the x_2 axis.

Table 3. Maximum sensitivity $\left|S_{\mathrm{m}}^{\mathrm{f}}\right|_{\max}$ for the Love mode devices based on different structures.

Basic structures	$\left\|S_{\mathrm{m}}^{\mathrm{f}}\right\|_{\max}$/$\mathrm{cm^2\cdot g^{-1}}$
CFEC/$[011]_c$ poled PZN-7%PT with the fibers parallel to the x_1 axis	1156
ZnO/90° ST-cut quartz[a)]	950
CFEC/$[011]_c$ poled PZN-7%PT with the fibers parallel to the x_2 axis	843
~1.55 μm PMMA/~2.2 μm SiO_2/quartz[b)]	640
SiO_2/90° ST-cut quartz[b)]	400

[a)]Refs. [4] and [5]. [b)]Refs. [3]–[5], [8] and [9].

Figures 7 and 8 show the relative scaled frequency sensitivity $\left|S_{\mathrm{m}}^{\mathrm{f}}\right|\lambda$ for the first-order mode with CFEC/PZN-xPT configuration with the carbon fibers parallel to the x_1 and x_2 axes, respectively. The peak data from Figs. 7 and 8 are listed in Tables 4 and 5, which revealed that the maximum sensitivity $\left(\left|S_{\mathrm{m}}^{\mathrm{f}}\right|\lambda\right)_{\max}$ increases with the elastic constant c_{66}^{E} for the $[011]_c$ poled PZN-xPT single crystal, while the optimal ratio $(h/\lambda)_{\mathrm{opt}}$ exhibits a decreasing tendency. For the $[001]_c$ and $[011]_c$ poled PZN-7%PT single crystals (the two elastic constants c_{66}^{E} are equal), the maximum sensitivity $\left(\left|S_{\mathrm{m}}^{\mathrm{f}}\right|\lambda\right)_{\max}$ exhibits an increasing tendency with decreasing density.

From Figs. 7 and 8 and Tables 4 and 5, one can find that the normalized maximum sensitivity $\left(\left|S_{\mathrm{m}}^{\mathrm{f}}\right|\lambda\right)_{\max}$ is strongly dependent on the elastic constant c_{66}^{E} of the substrate. Hence, it is important to select a substrate material that has a larger elastic constant c_{66}^{E} and lower density in order to maximize the sensitivity of the gravimetric sensor. We found that the normalized maximum sensitivity $\left(\left|S_{\mathrm{m}}^{\mathrm{f}}\right|\lambda\right)_{\max}$ increases with the decrease of $(h/\lambda)_{\mathrm{opt}}$, whether the carbon fibers parallel to the x_1 axis or x_2 axis. From the dispersion curves for the first-order mode, we found that the velocity increases with the decrease of h/λ as shown in Figs. 3 and 4. Because these PZN-xPT single crystals have almost equal density, the one with larger c_{66}^{E} possess higher shear wave velocity. Hence, among these crystals, the velocity values at the optimal designs have an increasing tendency with decreasing $(h/\lambda)_{\mathrm{opt}}$ as shown in Tables 4 and 5. It is clear that the frequency values at the optimal points have the same tendency for a fixed wavelength (e.g., 24 μm). While for a given thickness h the sensitivity can be raised by increasing the operation frequency in a specified sensor configuration,[3] therefore the increasing trend of $\left(\left|S_{\mathrm{m}}^{\mathrm{f}}\right|\lambda\right)_{\max}$ listed in Tables 4 and 5 happens because of the increased operation frequency.

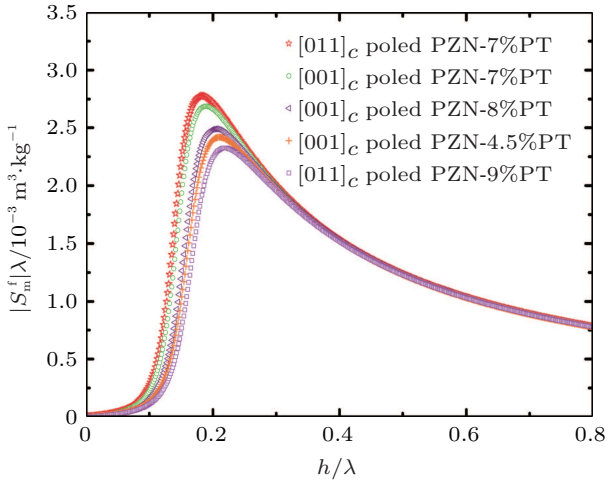


Fig. 7. (color online) Relative scaled frequency sensitivity $\left|S_{\mathrm{m}}^{\mathrm{f}}\right|\lambda$ for the first-order mode device with CFEC/PZN-(0.045–0.09)PT configuration with the carbon fibers parallel to the x_1 axis.

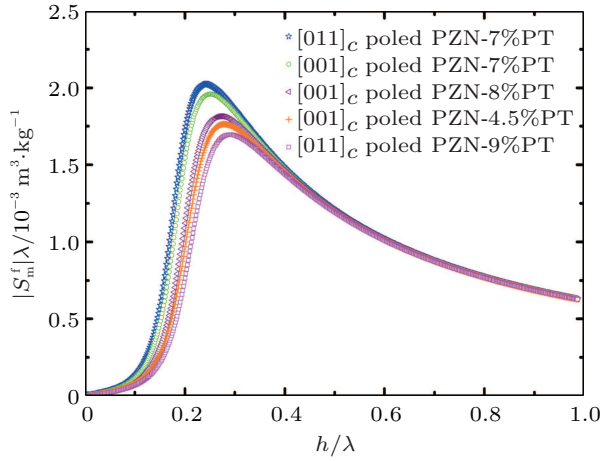


Fig. 8. (color online) Relative scaled frequency sensitivity $\left|S_{\mathrm{m}}^{\mathrm{f}}\right|\lambda$ for the first-order mode device with CFEC/PZN-(0.045–0.09)PT configuration with the carbon fibers parallel to the x_2 axis.

Table 4. Maximum relative scaled frequency sensitivity $\left(\left|S_{\mathrm{m}}^{\mathrm{f}}\right|\lambda\right)_{\max}$ and optimal design of normalized layer thickness (h/λ) for the first-order mode on CFEC/PZN-(4.5–9%)PT configurations with carbon fibers parallel to the x_1 axis.

Piezoelectric substrate	$(c_{66}^{\mathrm{E}}/10^{10}$ N·m$^{-2})$[a]	$(\left\|S_{\mathrm{m}}^{\mathrm{f}}\right\|\lambda)_{\max}/10^{-3}$ m^3·kg^{-1}	$(h/\lambda)_{\mathrm{opt}}$	$(\rho$/kg·m$^{-3})$[a]
$[011]_c$ poled PZN-7%PT	7.10	2.775	0.183	8038
$[001]_c$ poled PZN-7%PT	7.10	2.687	0.189	8350
$[001]_c$ poled PZN-8%PT	6.50	2.489	0.205	8315
$[001]_c$ poled PZN-4.5%PT	6.30	2.419	0.210	8310
$[011]_c$ poled PZN-9%PT	6.046	2.325	0.220	8316

[a] Refs. [13] and [20]–[22].

Table 5. Maximum relative scaled frequency sensitivity $\left(\left|S_{\mathrm{m}}^{\mathrm{f}}\right|\lambda\right)_{\max}$ and optimal design of normalized layer thickness (h/λ) for the first-order mode on CFEC/PZN-(4.5–9%)PT configurations with carbon fibers parallel to the x_2 axis.

Piezoelectric substrate	$(c_{66}^{\mathrm{E}}/10^{10}$ N·m$^{-2})$[a]	$(\left\|S_{\mathrm{m}}^{\mathrm{f}}\right\|\lambda)_{\max}/10^{-3}$ m^3·kg^{-1}	$(h/\lambda)_{\mathrm{opt}}$	$(\rho$/kg·m$^{-3})$[a]
$[011]_c$ poled PZN-7%PT	7.10	2.023	0.244	8038
$[001]_c$ poled PZN-7%PT	7.10	1.959	0.252	8350
$[001]_c$ poled PZN-8%PT	6.50	1.815	0.271	8315
$[001]_c$ poled PZN-4.5%PT	6.30	1.764	0.279	8310
$[011]_c$ poled PZN-9%PT	6.046	1.695	0.291	8316

[a] Refs. [13] and [20]–[22].

4. Summary and conclusions

Since the waveguide layer can be fabricated with different carbon proportions and with different carbon fiber orientations, one may use this advantage to optimize the density and elastic constants and enhance the directivity of acoustic waves guided for improving the performance of the device. Therefore, the CFEC is a very promising waveguide material and the high electromechanical coupling factor makes PZN-PT single crystals, particularly $[011]_c$ poled PZN-7%PT single crystals, ideal for making the substrate. By analyzing the gravimetric sensors made of PZN-xPT single crystals as the substrate, a general guideline for improving the sensor sensitivity, has been summarized: the substrate material should have larger elastic constant c_{66}^{E}, lower density, and higher shear velocity. It is obvious that we can obtain the best sensor sensitivity when the carbon fibers are parallel to the x_1 axis, namely the fibers along the direction of the wave propagation. This phenomenon happens because the acoustic wave is guided by the carbon fibers in waveguide material. Therefore, a better method is to adopt a unidirectional CFEC waveguide layer with the fibers parallel to the direction of the propagation of the acoustic wave.

References

[1] Tamarin O, Déjous C, Rebi'ere D, Pistré J Comeau S, Moynet D and Bezian J 2003 *Sens. Actuators B* **91** 275

[2] Moreira F, Hakiki M E, Sarry F, Brizoual L L, Elmazria O and Alnot P 2007 *IEEE Sensors J.* **7** 336

[3] Jakoby B and Vellekoop M J 1997 *Smart Mater. Struct.* **6** 668

[4] Zadeh K K, Trinchi A, Wlodarski W and Holland A 2002 *Sens. Actuators A* **100** 135

[5] Zadeh K K, Trinchi A, Wlodarski W, Chen Y Y, Fry B N and Galatsis K 2003 *Sens. Actuators B* **91** 143

[6] Schlensog M D, Gronewold T M A, Tewes M, Famulok M and Quandt E 2004 *Sens. Actuators B* **101** 308

[7] Wang Z, Cheeke J D N and Jen C K 1994 *Appl. Phys. Lett.* **64** 2940

[8] Du J and Harding G L 1998 *Sens. Actuators A* **65** 152

[9] Liu J S and He S T 2010 *J. Appl. Phys.* **107** 073511

[10] Wang Y L, Zhang R, Sun E W, Song W and Cao W W 2013 *Chin. Phys. Lett.* **30** 096301

[11] Park S E and Shrout T R 1997 *J. Appl. Phys.* **82** 1804

[12] Zhu H B, Wu Z B and Liu G Q, Xi K, Li S S and Dong Y Y 2013 *Acta Phys. Sin.* **62** 014205 (in Chinese)

[13] Zhang R, Jiang B, Jiang W H and Cao W W 2006 *Appl. Phys. Lett.* **89** 242908

[14] Huang N X, Lú T Q, Zhang R and Cao W W 2013 *Appl. Phys. Lett.* **103** 053507

[15] Chen C W, Zhang R, Chen H and Cao W W 2007 *Appl. Phys. Lett.* **91** 102907

[16] Nayfeh A H and Chien H T 1992 *J. Acoust Soc. Am.* **91** 1250

[17] Yang C H and Chimenti D E 1993 *Appl. Phys. Lett.* **63** 1328

[18] Yang C H and Chimenti D E 1995 *J. Acoust. Soc. Am.* **97** 2103

[19] Farnell G W and Adler E L 1972 *Physical Acoustics*, edited by Mason W P and Thurston R N (Vol. **IX**) (New York: Academic) pp. 35–127

[20] Yin J H, Jiang B and Cao W W 2000 *IEEE Trans. Ultrason. Ferroelectr. Freq. Control.* **47** 285

[21] Zhang R, Jiang B and Cao W W 2002 *J. Mater. Sci. Lett.* **21** 1877

[22] He C J, Jing W P, Wang F F, Zhu K J and Qiu J H 2011 *IEEE Trans. Ultrason. Ferroelectr. Freq. Control.* **58** 1127

[23] Potel C, Baly S, de Belleval J F, Lowe M and Gatignol P 2005 *IEEE Trans. Ultrason. Ferroelectr. Freq. Control.* **52** 987

[24] Auld B A 1976 *Acoustic Fields and Waves in Solids* (Vol. **2**) (New York: Wiley) pp. 271–332